

Article

Probing Attosecond Electron Coherence in Molecular Charge Migration by Ultrafast X-Ray Photoelectron Imaging

Kai-Jun Yuan *  and André D Bandrauk *Laboratoire de Chimie Théorique, Faculté des Sciences, Université de Sherbrooke,
Sherbrooke, QC J1K 2R1, Canada

* Correspondence: kaijun.yuan@usherbrooke.ca (K.-J.Y.); andre.bandrauk@usherbrooke.ca (A.D.B.)

Received: 5 April 2019; Accepted: 7 May 2019; Published: 11 May 2019



Abstract: Electron coherence is a fundamental quantum phenomenon in today's ultrafast physics and chemistry research. Based on attosecond pump–probe schemes, ultrafast X-ray photoelectron imaging of molecules was used to monitor the coherent electron dynamics which is created by an XUV pulse. We performed simulations on the molecular ion H_2^+ by numerically solving time-dependent Schrödinger equations. It was found that the X-ray photoelectron angular and momentum distributions depend on the time delay between the XUV pump and soft X-ray probe pulses. Varying the polarization and helicity of the soft X-ray probe pulse gave rise to a modulation of the time-resolved photoelectron distributions. The present results provide a new approach for exploring ultrafast coherent electron dynamics and charge migration in reactions of molecules on the attosecond time scale.

Keywords: electron coherence; charge migration; soft X-ray attosecond pulse; time-resolved photoelectron imaging

1. Introduction

Time-resolved photoelectron emission spectroscopy has been used widely as an efficient technique for investigating nuclear and electronic dynamics in molecular reactions [1–8]. An ultrashort pump laser pulse initiates a coherent transition between ground and excited states in molecules and the time evolution is subsequently monitored after a variable time delay by a second probe pulse. Advances in synthesizing ultrashort intense pulses [9–11] allow one to visualize and control molecular reaction processes from femtosecond ($1 \text{ fs} = 10^{-15} \text{ s}$) time scales for nuclear vibrations to attosecond ($1 \text{ as} = 10^{-18} \text{ s}$) scales for electron motion. Currently, the shortest attosecond pulses with a duration of 43 as are available for such new photoelectron imaging techniques [12]. Electrons have a great potential for probing the time-resolved transient structure of matter via ultrashort photoelectron spectroscopy. One now can envisage the emergence of laser-induced electron interference and diffraction [13–20] as efficient methods of measuring molecular electronic structure and electron motion for different fixed nuclear configurations.

Recently, ultrafast charge migration arising from a coherent population excitation in multiple electronic states has attracted considerable attention in the field of photophysics and photochemistry [21–35]. It has been shown that quantum control of electron flux during intramolecular charge migration can be produced by designing ultrafast laser pulse that prepare the system in selective electronic state [36–38]. The electron currents are sensitive to the polarization and helicity of the driving pulse, i.e., the symmetry of the excited electronic state [39]. Recent work has shown how to control molecular electric symmetry via charge migration with ultrashort laser [40,41]. By measuring

high-order harmonic generation in ionized iodoacetylene via attosecond electron recollision, one can probe attosecond charge migration [42]. Angular electronic fluxes can also be used to reconstruct electron charge migration in excited benzene by preparing a coherent electronic state [37,39], which can be monitored in photoelectron momentum spectra by a time-delayed high frequency attosecond pulses [43]. It is also found that molecular photoelectron angular distributions depend on the symmetry of molecular orbitals and molecular bondings, thus allowing to monitor electron coherent and charge migration [44–47]. Most recently, nonresonant ultrafast X-ray scattering from a molecular wave packet has been used to observe an adiabatic electron transfer in molecules [48].

Time-resolved photoelectron imaging as a variant of time-resolved photoelectron spectroscopy has been used to study molecular dynamics [49,50]. In the present work, we theoretically studied time resolved photoelectron emission with attosecond resolutions in molecular coherent excitation and charge migration processes. A coherent superposition of quantum states was created by a linearly polarized XUV pump pulse. Subsequently, a time delayed soft X-ray pulse was used to ionize the excited molecules, as illustrated in Figure 1. Simulations were performed on the benchmark molecular ion H_2^+ by numerically solving the corresponding time-dependent Schrödinger equation (TDSE). Results show that photoelectron momentum distributions exhibit asymmetric structure and evolve periodically with time, reflecting the electron coherence in molecular charge migration. It was found that the evolution of the photoelectron distributions is dependent on the polarization and helicity of the probe pulse.

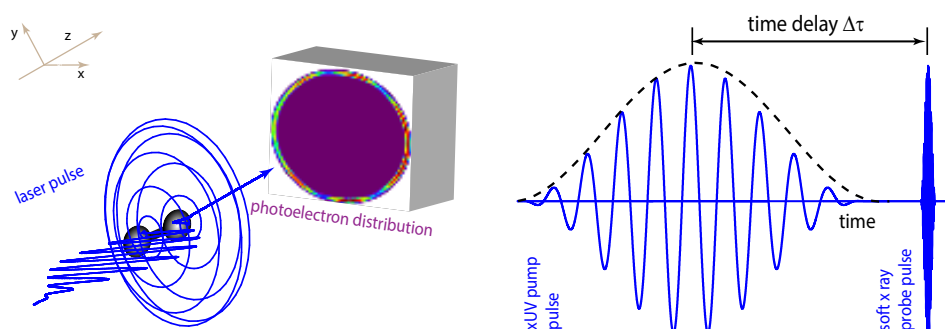


Figure 1. Illustration of time-resolved photoelectron imaging of coherent electron excitation in molecules by an XUV pump pulse and a time delayed soft X-ray probe pulse. The molecule H_2^+ is aligned along the z-axis and the pump–probe pulses with their field vectors in the (x, y) plane propagate along the z-axis. The time delay $\Delta\tau$ is the time interval between the peak times of the pump and probe pulses.

The paper is arranged as follows: In Section 2, we briefly describe the computation methods. The numerical results obtained by time-dependent quantum electron wave-packet calculations from the corresponding TDSE for a prealigned H_2^+ are presented and discussed in Section 3. We describe the coherent excitation in molecules and analyze probing photoelectron angular and momentum distributions for imaging attosecond charge migration. Finally, we summarize our findings in Section 4 (throughout this paper, atomic units (a.u.) are used unless otherwise noted).

2. Numerical Methods

We briefly describe the numerical and computational methods for simulating the photoelectron emission process in aligned H_2^+ by pump–probe pulses, as illustrated in Figure 1. The corresponding three-dimensional (3D) TDSE within static nuclear frames reads as,

$$i\frac{\partial}{\partial t}\psi(\mathbf{r},t) = \left[-\frac{1}{2}\nabla_{\mathbf{r}}^2 + V_{en}(\mathbf{r}) + V_L(\mathbf{r},t) \right] \psi(\mathbf{r},t). \quad (1)$$

We describe the electron dynamics in cylindrical coordinates $\mathbf{r} = (\rho, \theta, z)$ with $x = \rho \cos \theta$ and $y = \rho \sin \theta$. Then, the kinetic (Laplacian) operator gives

$$-\frac{1}{2}\nabla_{\mathbf{r}}^2 = -\frac{1}{2\rho}\frac{\partial}{\partial\rho}\left(\rho\frac{\partial}{\partial\rho}\right) - \frac{1}{2\rho^2}\frac{\partial^2}{\partial\theta^2} - \frac{1}{2}\frac{\partial^2}{\partial z^2}. \tag{2}$$

V_{en} is the electron-nuclear potential. The molecule is aligned along the z -axis. The pump and probe laser pulses propagate along the z -axis, parallel to the molecular axis. The radiative interaction between the laser field and the electron $V_L(\mathbf{r}) = \mathbf{r} \cdot \mathbf{E}(t)$ is described in the length gauge. The total fields $\mathbf{E}(t) = \mathbf{E}_{pu}(t) + \mathbf{E}_{pr}(t)$ have the forms,

$$\mathbf{E}_{pu}(t) = \hat{e}_x E_0 f(t) \cos(\omega_{pu}t), \tag{3}$$

for a linearly polarized pump pulse with its field vector along the x -axis, and

$$\mathbf{E}_{pr}(t) = E_0 f(t) \begin{cases} \hat{e}_x \cos(\omega_{pr}t) \\ \hat{e}_y \xi \sin(\omega_{pr}t) \end{cases}, \tag{4}$$

for a circularly polarized probe pulse with its field vector in the (x, y) plane. The symbol $\xi = \pm 1$ denotes the helicity of the probe field, i.e., right ($\xi = +1$) or left ($\xi = -1$) handed circular polarization and $\xi = 0$ presents the linear polarization. A smooth $\sin^2(\pi t/T_{pu/pr})$ pulse envelope $f(t)$ for maximum amplitude E_0 , intensity $I_0 = I_x = I_y = c\epsilon_0 E_0^2/2$ and duration $T_{pu/pr} = 10\tau_{pu/pr}$ are used, where one optical cycle period $\tau_{pu/pr} = 2\pi/\omega_{pu/pr}$. This pulse satisfies the total zero area $\int E_{pu/pr}(t)dt = 0$ in order to exclude static field effects [9].

The 3D TDSE in Equation (1) for aligned H_2^+ is numerically solved by a second-order split operator method that conserves unitarity in the time step δt combined with a fifth order finite difference method and Fourier transform technique in the spatial steps $\delta\rho$, δz , and $\delta\theta$ [51,52]. The initial electron wavefunction $\psi(\mathbf{r}, t = 0)$ is prepared in the ground $1s\sigma_g$ state calculated by propagating an initial appropriate wavefunction in imaginary time using the zero-field TDSE in Equation (1). The time step is taken to be $\delta t = 0.01$ a.u. = 0.24 as. The spatial discretization is $\delta\rho = \delta z = 0.25$ a.u. for a radial grid range $0 \leq \rho \leq 128$ a.u. (6.77 nm) and $|z| \leq 32$ a.u. (1.69 nm), and the angle grid size $\delta\theta = 0.025$ radian. One notes that reflections of the electron wave packet from the edges of the numerical grid can cause artificial effects [53,54]. To prevent these unphysical effects, we multiply $\psi(\rho, \theta, z, t)$ by a mask function or absorption potential in the radial coordinates ρ with the form $\cos^{1/8}[\pi(\rho - \rho_a)/2\rho_{abs}]$. The important ultrafast electron dynamics in intense fields occur on a spatial volume close to the molecule. These studies can therefore be performed on a relatively small grid neglecting the exact form of the outgoing ionizing parts of the wave function. For all results reported here, we set the absorber domain at $\rho_a = \rho_{max} - \rho_{abs} = 104$ a.u. with $\rho_{abs} = 24$ a.u., exceeding well the field induced electron oscillation $\alpha_d = E_0/\omega_{pu/pr}^2$ of the electron.

Molecular frame photoelectron distributions are calculated by a Fourier transform of the 3D time dependent electronic wavefunction $\psi(\rho, \theta, z, t)$, which exactly describe the electron dynamics in the continuum [55,56]:

$$\begin{aligned} \mathcal{J}_l(\theta, z, E)|_{\rho_f} &= \int_{t_p}^{\infty} \psi(\theta, z, t)|_{\rho_f} e^{iEt} dt, \\ \mathcal{J}_r(\theta, z, E)|_{\rho_f} &= \int_{t_p}^{\infty} \frac{\partial\psi(\theta, z, t)}{\partial\rho}|_{\rho_f} e^{iEt} dt, \\ \mathcal{J}(\theta, E) &\sim \text{Re} \left[\frac{1}{2i} \int \mathcal{J}_l^*(\theta, z, E)|_{\rho_f} \mathcal{J}_r(\theta, z, E)|_{\rho_f} dz \right], \end{aligned} \tag{5}$$

where t_p is the time after the pulse turns off and $\rho_f = 100$ a.u. is an asymptotic point before the wavepacket is absorbed. $E = p_e^2/2$ is the kinetic energy of an ionized electron with wave vector

$k = p_e = 2\pi/\lambda_e$, $p_e = (p_x^2 + p_y^2)^{1/2}$ is the momentum of a photoelectron of wavelength λ_e . Since the ionization occurs in the laser polarization (x, y) molecular plane, we define θ as the angle between the electron momentum \mathbf{p}_e and the x polarization axis. With the transformation $p_x = p_e \cos \theta$ and $p_y = p_e \sin \theta$, we then obtain the two-dimensional (2D) momentum distributions of photoelectrons from Equation (5). Molecular photoelectron angular distributions at photoelectron kinetic energy E_e are obtained by integrating over the one photon energy, where the spectral width of the probe pulse $\Delta\omega \approx \omega_{pr}/3$,

$$\mathcal{J}^{E_e}(\theta) = \int_{E_e - \omega_{pr}/3}^{E_e + \omega_{pr}/3} dE \mathcal{J}(\theta, E), \tag{6}$$

corresponding to the main one photon ω_{pr} frequency of absorption.

3. Results and Discussions

We use the molecule H_2^+ as a benchmark system, which can be fully investigated [57] to describe the photoelectron imaging process of coherent electron dynamics. The molecule at equilibrium aligned along the z -axis is excited by a linearly polarized $\lambda_{pu} = 70$ nm XUV pump laser pulse with its field vector along the x -axis. Subsequently, a $\lambda_{pr} = 5$ nm soft X-ray attosecond probe pulse with its field vector polarized in the (x, y) plane ionizes the excited molecule. For the processes by high-frequency pump–probe pulses, multi-photon ionization dominates with the Keldysh parameter $\gamma \gg 1$ [9]. Since the ponderomotive energy $U_p = E_0^2/4\omega_{pr}^2$ is very weak, the modification of the ionization potential by laser induced Stark shifts can be ignored as well. Moreover, the dipole approximation, in which the spatial dependence and magnetic component of the external field are neglected, remains valid.

We first present the coherent excitation and charge migration by a pump pulse. With a linearly polarized pump pulse with its field vector polarized along x -axis, perpendicular to the molecular axis, a $\sigma_g - \pi_u$ parallel resonant pump excitation occurs from the electronic ground $1s\sigma_g$ state, $\psi_{\sigma_g}(\mathbf{r})$ with the eigenenergy E_{σ_g} to the electronic excited $2p\pi_u$ state, $\psi_{\pi_u}(\mathbf{r})$ with the eigenenergy E_{π_u} . In our numerical models, the energies for the $1s\sigma_g$ and $2p\pi_u$ states are, respectively, $E_{\sigma_g} = -1.08$ a.u. and $E_{\pi_u} = -0.43$ a.u. To induce molecular resonant excitation, the wavelength $\lambda_{pu} = 70$ nm ($\omega_{pu} = 0.65$ a.u.) of the pump pulse is required, where $\omega_{pu} = E_{\pi_u} - E_{\sigma_g} = 0.65$ a.u. A coherent superposition of the two electronic states is then created due to a strong charge-resonance excitation [58],

$$\psi_0(\mathbf{r}, t) = c_{\sigma_g}(t)\psi_{\sigma_g}(\mathbf{r})e^{-iE_{\sigma_g}t} + c_{\pi_u}(t)\psi_{\pi_u}(\mathbf{r})e^{-iE_{\pi_u}t}. \tag{7}$$

$c_{\sigma_g}(t)$ and $c_{\pi_u}(t)$ are the occupation coefficients. $\psi_{\pi_u}(\mathbf{r})$ is the degenerate quantum electronic state. For the case excited by the linearly polarized 70 nm XUV laser pulse with its vector along the x -axis, the wavefunction of the degenerate excited state is given by [59],

$$\psi_{\pi_u}(\mathbf{r}) = [\psi_{\pi_u}^+(\mathbf{r}) + \psi_{\pi_u}^-(\mathbf{r})]/\sqrt{2}. \tag{8}$$

By describing the electronic motions in the cylindrical coordinate space with $\mathbf{r} = (\rho, \theta, z)$ with ($x = \rho \cos \theta, y = \rho \sin \theta$) and aligning the molecule along the z -axis, the wave function of the degenerate excited state can be written as

$$\psi_{\pi_u}^{\pm}(\rho, z) = \tilde{\psi}_{\pi_u}^{\pm}(\rho, z) \exp(\pm i\theta), \tag{9}$$

where $|\tilde{\psi}_{\pi_u}^{\pm}(\rho, z)|^2 = [|\psi_{\pi_u}^x(\rho, z)|^2 + |\psi_{\pi_u}^y(\rho, z)|^2]/2$, and $|\psi_{\pi_u}^x(\rho, z)|^2$ and $|\psi_{\pi_u}^y(\rho, z)|^2$ are the degenerate real orbitals. The electron density distribution of the coherent superposition electronic state in Equation (7) is described by,

$$\begin{aligned}
\mathcal{P}(\mathbf{r}) &= |\psi_0(\mathbf{r}, t)|^2 \\
&= |c_{\sigma_g}(t)|^2 |\psi_{\sigma_g}(\rho, z)|^2 + |c_{\pi_u}(t)|^2 |\tilde{\psi}_{\pi_u}^{\pm}(\rho, z)|^2 \\
&\quad + 2|c_{\sigma_g}(t)||c_{\pi_u}(t)| |\psi_{\sigma_g}(\rho, z)\tilde{\psi}_{\pi_u}^{\pm}(\rho, z) \cos(\Delta Et) \cos(\theta)|.
\end{aligned} \tag{10}$$

The coherent electron dynamics is composed of two electronic state densities, $\mathcal{P}^{(g)}(\mathbf{r}) = |c_{\sigma_g}(t)|^2 |\psi_{\sigma_g}(\mathbf{r})|^2$ and $\mathcal{P}^{(u)}(\mathbf{r}) = |c_{\pi_u}(t)|^2 |\psi_{\pi_u}(\mathbf{r})|^2$, and their interfering superposition $\mathcal{P}^{(g,u)}(\mathbf{r}, t) = 2|c_{\sigma_g}(t)||c_{\pi_u}(t)| |\psi_{\sigma_g}(\mathbf{r})\psi_{\pi_u}(\mathbf{r}) \cos(\Delta Et) \cos(\theta)|$. After the pump pulse, the occupation coefficients $c_{\sigma_g}(t)$ and $c_{\pi_u}(t)$ are constant and $\mathcal{P}^{(g)}(\mathbf{r})$ and $\mathcal{P}^{(u)}(\mathbf{r})$ are symmetric and are insensitive to the time, whereas the coherent superposition term $\mathcal{P}^{(g,u)}(\mathbf{r})$ is determined by the time t and the angle θ . Note that, for the linear polarization resonant excitation, the distribution of the coherent superposition term is mainly along the laser polarization direction with a function $\cos(\theta)$.

Figure 2 shows numerical results of electron density distributions $\mathcal{P}(x, y)$ of the superposition state created by the $\lambda_{pu} = 70$ nm ($\omega_{pu} = 0.65$ a.u.) pump pulse as a function of the time t , where $\mathcal{P}(x, y) = \int dz |\psi^2(x, y, z)|^2$ in Equation (1). We use the pulse intensity $I_0 = 1.0 \times 10^{14}$ W/cm² ($E_0 = 5.34 \times 10^{-2}$ a.u.), and durations $T_{pu} = 10\tau_{pu} = 2.32$ fs (1.16 fs full width at half maximum, FWHM). Of note is that the occupation coefficients, $c_{\sigma_g}(t)$ and $c_{\pi_u}(t)$, are dependent on the intensity of the pump pulse. Varying I_0 leads to a variance of the electron coherence in Equation (7). At such intensity $I_0 = 1.0 \times 10^{14}$ W/cm², one obtains the maximum interference effects. After the pump pulse, the occupation coefficients are constant. Figure 2 shows that the electron density distributions $\mathcal{P}(x, y)$ are asymmetric with respect to the molecular center and oscillate with the time t . The coherent electron wave packets move periodically in the left ($x < 0$) and right ($x > 0$) half planes along the laser x polarization axis. At time $t = 9.75\tau_{pu}$, the coherent electron wave packets are mainly localized in the left plane of the molecule. As the time t increases, the electron moves to the right. At time $t = 10.25\tau_{pu}$, the density distributions of the coherent electron wave packets lie in the right plane. As the time t increases further, the electron wave packets come back to the left plane.

The evolution of the electron density distributions in Figure 2 describes the dependence of the attosecond electron coherence on the time t in charge migration, i.e., the superposition term $\mathcal{P}^{(g,u)}(\mathbf{r})$ in Equation (10). The period of the oscillation is $\tau = \tau_{pu} = 232$ as for the time t , in good agreement with the prediction in Equation (10). Since $\mathcal{P}^{(g,u)}(\mathbf{r}) \sim \cos(\Delta Et) \cos(\theta)$, the density distributions of the coherent electron wave packets are asymmetric along the x -axis and the extreme value occurs at $\theta = 0$ or π (180°). Varying the time t leads to a modulation of the coherent electron density distribution following a form $\cos(\Delta Et)$. The time dependent electron density distributions reflects the electron coherence.

To visualize the coherent electron wave packets in Figure 2, we present the process of time resolved photoelectron imaging by pump–probe pulses. Because the oscillation period of the coherent electron is very short, $\tau = 232$ as, a soft X-ray attosecond probe pulse is necessary. We use a $\lambda_{pr} = 5$ nm ($\omega_{pr} = 9.11$ a.u.) and $T_{pr} = 10\tau_{pr}$ (83 as FWHM) probe pulse to ionize the excited molecule prepared by the linearly x polarized $\lambda_{pu} = 70$ nm pump pulse in Figure 2. The use of the soft X-ray pulse has the following advantage in probing the electronic coherence. First the high frequency single photon process can avoid additional excitation effects resulting from other lower electronic states. Second, the extremely short duration of the X-ray pulse on the attosecond time scale can be utilized to resolve the coherent electron rotation with the period of a few hundred attoseconds. Figure 3 displays molecular photoelectron momentum $\mathcal{J}(p_x, p_y)$ and angular $\mathcal{J}(\theta)$ distributions produced by a linearly polarized $\lambda_{pr} = 5$ nm attosecond probe pulse with its field vector along the x -axis, i.e., $\xi = 0$. The time delay $\Delta\tau$ between the pump and probe pulses varies from $\Delta\tau = 4.75\tau_{pu}$ to $6.0\tau_{pu}$ with a time interval of $0.25\tau_{pu}$. The other laser parameters are always fixed at pulse intensities $I_0 = 1.0 \times 10^{14}$ W/cm² ($E_0 = 5.34 \times 10^{-2}$ a.u.) and durations $T_{pu} = 10\tau_{pu} = 2.32$ fs (1.16 fs FWHM) and $T_{pr} = 10\tau_{pr} = 165.4$ as (83 as FWHM). The proper intensity of the probe pulse should be chosen. With lower intensities of the X-ray pulse, the probing photoelectron signal will be weak due to small transition dipole moments,

whereas, with very strong intensities, the broad spectral width of the X-ray pulse will induce additional unexpected strong field phenomena. Since we focus on the probing photoelectron emission produced by the soft X-ray pulse, only the photoelectron distributions around the momentum $p_e = 4.01$ a.u., where $p_e = \pm\sqrt{2(\omega_{pr} - I_p)}$ corresponds to one ω_{pr} photon absorption, are presented in Figure 3. The angular distributions calculated in Equation (6) are also displayed.

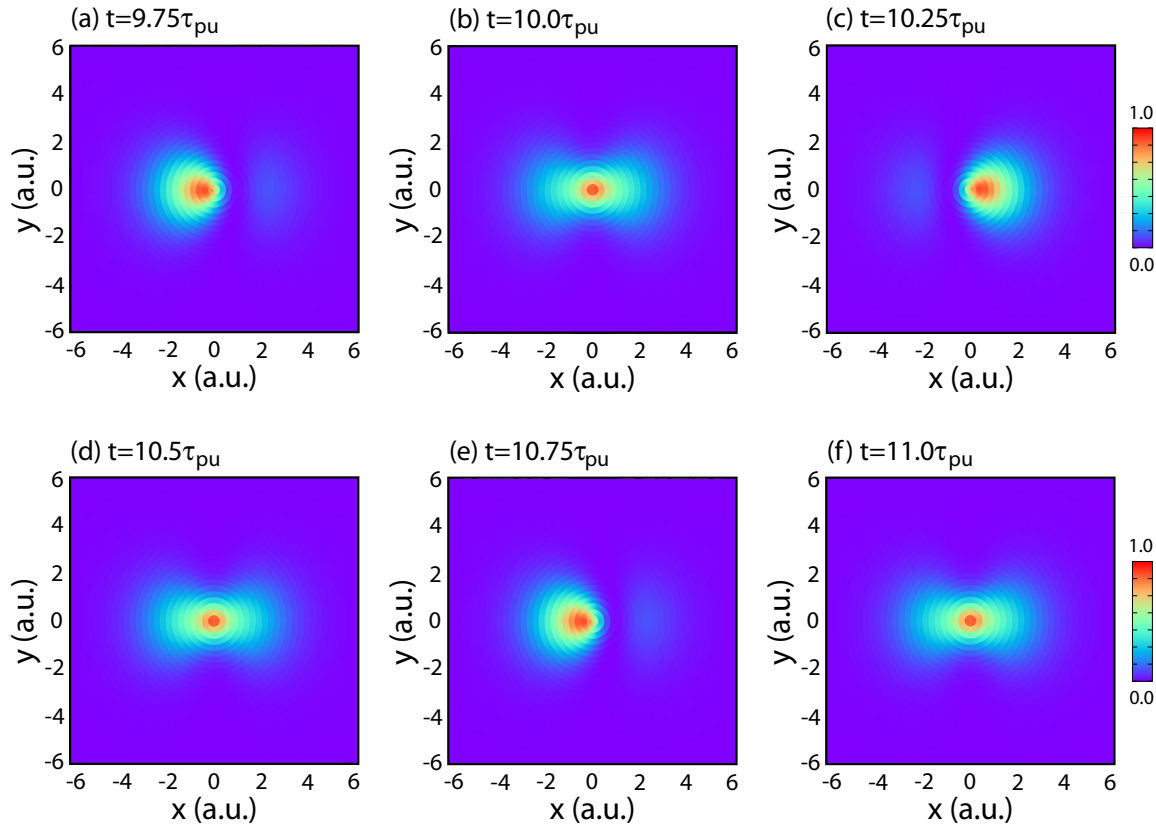


Figure 2. Evolution of the electron density probabilities $\mathcal{P}(x, y)$ with the time t in the molecular ion H_2^+ aligned along the z -axis excited by a linearly polarized $\lambda = 70$ nm pump pulse with its field vector along the x -axis at intensity $I_0 = 1.0 \times 10^{14}$ W/cm² ($E_0 = 5.34 \times 10^{-2}$ a.u.) and duration $T = 10\tau_{pu} = 2.32$ fs.

Figure 3 shows that asymmetric photoelectron angular and momentum distributions are produced, which are shown to be dependent on the time delay $\Delta\tau$. Altering the time delay $\Delta\tau$ results in a change of the asymmetry. At $\Delta\tau = 4.75\tau_{pu}$, the distributions in the right half angular and momentum plane dominate. Increasing $\Delta\tau$ leads to a decrease of the right momentum ring and an increase of the left in amplitude. At $\Delta\tau = 5.0\tau_{pu}$ the amplitudes of the momentum distributions in the left and half planes are comparable, and at $\Delta\tau = 5.25\tau_{pu}$ the left one reaches the maximum value. Increasing the time delay $\Delta\tau$ further, a reverse process occurs where the left distribution decreases while the right one increases. At $\Delta\tau = 5.5\tau_{pu}$, the comparable distributions in the left and right planes are obtained, and at $\Delta\tau = 5.75\tau_{pu}$, the right one dominates again. The periodical evolution of the photoelectron momentum distributions with the time delay $\Delta\tau$ illustrates the electronic coherence in the resonant excitation by the pump pulse. The evolution period is $\tau = \tau_{pu} = 2\pi/\Delta E$, the same as the coherent electron wave packets in Equation (10) and Figure 2. The electronic coherence gives rise to asymmetric electron density distributions of the coherent superposition state $\psi_0(\mathbf{r}, t)$.

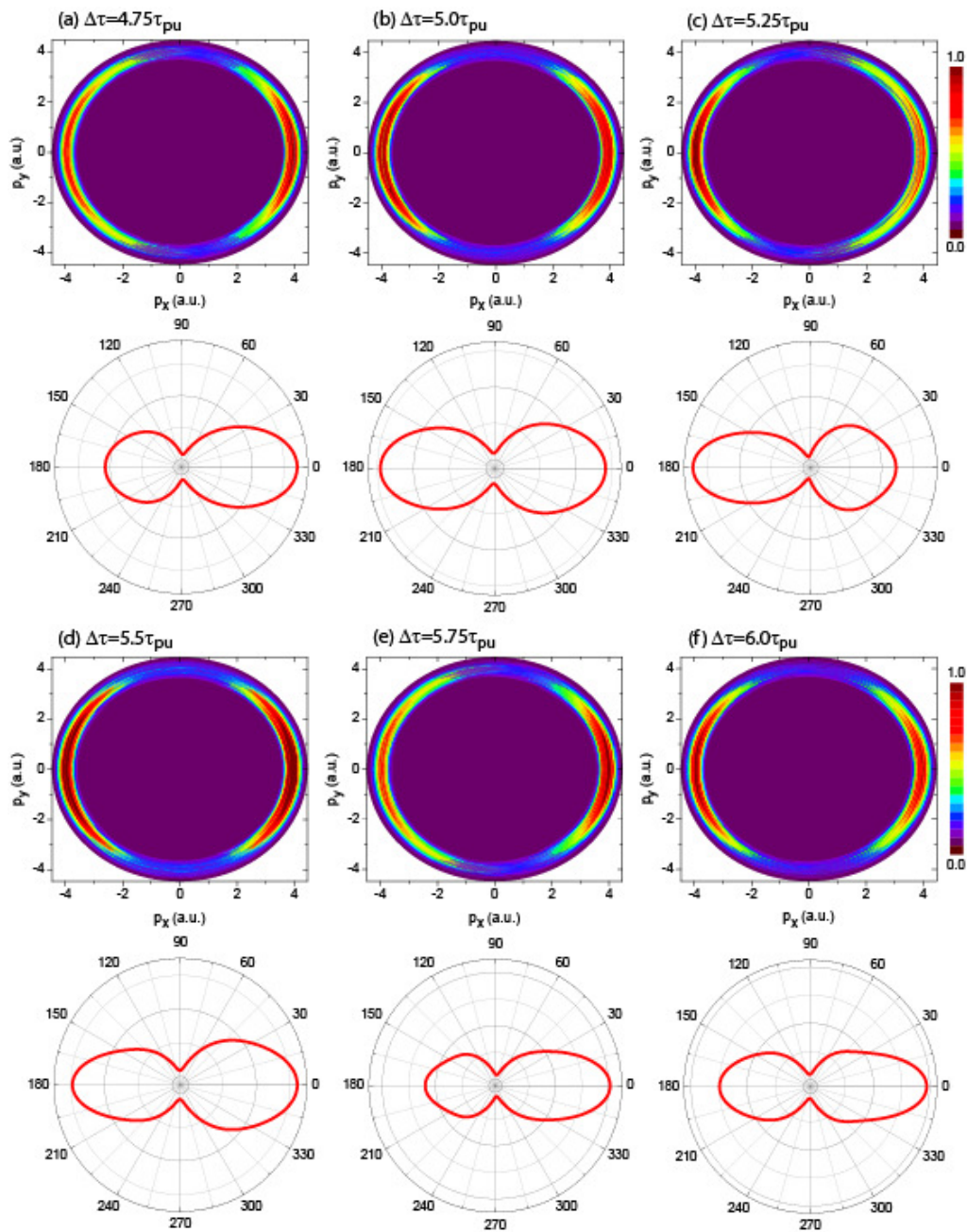


Figure 3. Evolutions of photoelectron momentum $\mathcal{J}(p_x, p_y)$ and angular $\mathcal{J}(\theta)$ distributions as a function of the time delay $\Delta\tau$ between the linearly polarized $\lambda_{pu} = 70$ nm pump and $\lambda_{pr} = 5$ nm probe pulses with their field vectors polarized along the x -axis. The time delays are: (a) $\Delta\tau = 4.75\tau_{pu}$; (b) $5.0\tau_{pu}$; (c) $5.25\tau_{pu}$; (d) $5.5\tau_{pu}$; (e) $5.75\tau_{pu}$; and (f) $6.0\tau_{pu}$. The molecule H_2^+ is aligned along the z -axis. The pulse intensities $I_0 = 1.0 \times 10^{14}$ W/cm² ($E_0 = 5.34 \times 10^{-2}$ a.u.) and duration $T_{pu} = 10\tau_{pu} = 2.32$ fs (1.16 fs FWHM) and $T_{pr} = 10\tau_{pr} = 165.4$ as (83 as FWHM) are always fixed.

The polarization of the probe pulse can influence the probing photoelectron imaging of the coherent electron dynamics. We next present the photoelectron imaging process by a circularly polarized probe laser pulse. Figure 4 shows results of photoelectron momentum $\mathcal{J}(p_x, p_y)$ distributions by a left-handed $\zeta = -1$ circularly polarized $\lambda_{pr} = 5$ nm probe pulse. The corresponding photoelectron angular $\mathcal{J}(\theta)$ distributions obtained from Equation (6) are also plotted (yellow curves). We use again a linearly polarized $\lambda_{pu} = 70$ nm pump pulse with its field vector polarized along the x -axis to excited the molecule H_2^+ aligned along the z -axis, the same as in Figures 2 and 3. We show the helicity effects of the probe pulse on the photoelectron angular and momentum distributions of the coherent excitation.

The pulse intensities $I_0 = 1.0 \times 10^{14}$ W/cm² ($E_0 = 5.34 \times 10^{-2}$ a.u.) and duration $T_{pu} = 10\tau_{pu} = 2.32$ fs (1.16 fs FWHM) and $T_{pr} = 10\tau_{pr} = 165.4$ as (83 as FWHM) are always fixed while the time delay $\Delta\tau$ between the pump–probe pulse varies from $4.75\tau_{pu}$ to $6.0\tau_{pu}$.

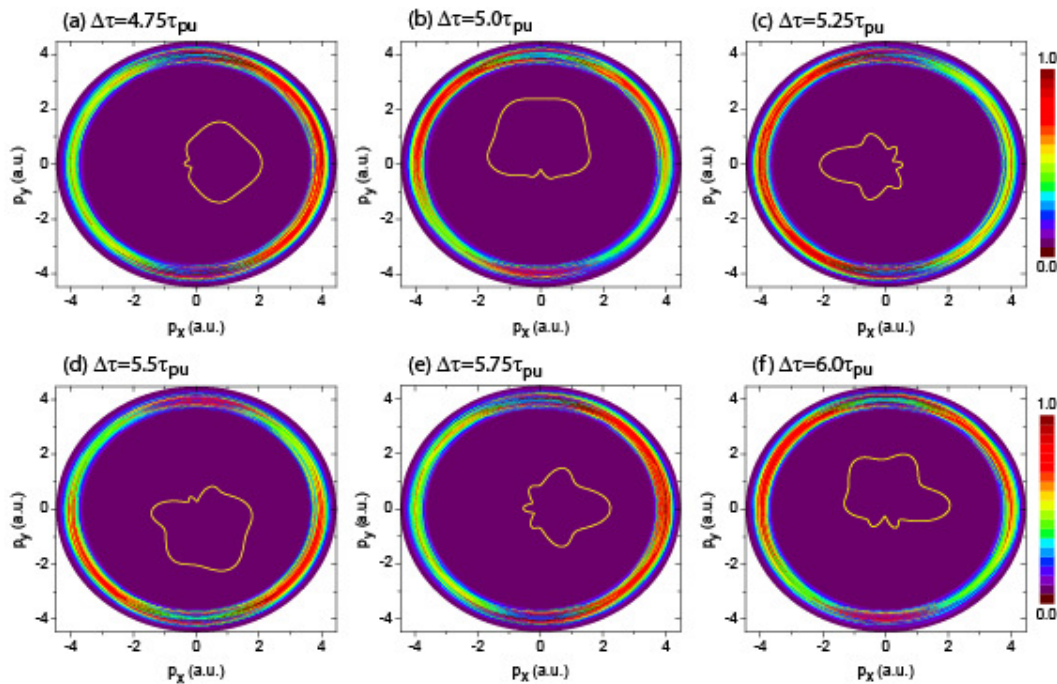


Figure 4. 2D Photoelectron momentum $\mathcal{J}(p_x, p_y)$ distributions as a function of the time delay $\Delta\tau$ between the linearly x polarized $\lambda_{pu} = 70$ nm pump pulse and the circularly (x, y) polarized $\lambda_{pr} = 5$ nm probe pulse with left-handed helicity $\zeta = -1$. The time delay $\Delta\tau$ varies: (a) $\Delta\tau = 4.75\tau_{pu}$; (b) $5.0\tau_{pu}$; (c) $5.25\tau_{pu}$; (d) $5.5\tau_{pu}$; (e) $5.75\tau_{pu}$, and (f) $6.0\tau_{pu}$. The molecule H_2^+ is aligned along the z -axis. The pulse intensities $I_0 = 1.0 \times 10^{14}$ W/cm² ($E_0 = 5.34 \times 10^{-2}$ a.u.) and duration $T_{pu} = 10\tau_{pu} = 2.32$ fs (1.16 fs FWHM) and $T_{pr} = 10\tau_{pr} = 165.4$ as (83 as FWHM) are always fixed. Inserts (yellow curves) are photoelectron angular $\mathcal{J}(\theta)$ distributions obtained from Equation (6).

Figure 4 shows that asymmetric photoelectron angular and momentum distributions are produced again which evolve periodically with the time delay $\Delta\tau$. Comparing to the process by a linearly polarized probe pulse in Figure 3, the time resolved photoelectron distributions rotate periodically with an anti-clockwise direction around the molecular R or z -axis. As shown in Figure 4a at $\Delta\tau = 4.75\tau_{pu}$, the photoelectron distributions are mainly localized in the right half plane. As the time delay $\Delta\tau$ increases, the distribution rotate to the upper half plane ($p_y > 0$) and then to the left. At $\Delta\tau = 5.5\tau_{pu}$, the photoelectron distributions in the lower half plane ($p_y < 0$) dominate. At $\Delta\tau = 5.75\tau_{pu}$ the distributions move back to the right. The evolution period of the photoelectron distributions is $\tau_{pu} = 2\pi/\Delta E = 232$ as, as predicted in Equation (10) for the coherent electronic wave packets.

The rotation of the probing photoelectron distributions with the time delay $\Delta\tau$ corresponds to the helicity of the probe pulses. For the circularly polarized probe pulse, its field vector is isotropic in the (x, y) polarization plane. Moreover, for the molecule H_2^+ aligned along the z -axis, the influence of the molecular potential on the high frequency photoelectron emission is negligible. As a result, the asymmetric photoelectron distributions are determined by the electric field vector of the probe pulse, leading to a rotation around the molecular axis. That differs from the linear probe process in Figure 3 where the photoelectron distributions are mainly localized along the laser polarization direction since the field-molecule interaction term follows the form $\cos(\theta)$, i.e., $\sim \mathbf{r} \cdot \mathbf{E}$.

We finally show the effect of the helicity of the circularly polarized probe pulse on the photoelectron emission. Figure 5 displays results of photoelectron momentum $\mathcal{J}(p_x, p_y)$ and angular $\mathcal{J}(\theta)$ distributions with right handed helicity $\zeta = 1$. The other laser parameters are the same as those

used in Figure 4. Figure 5 shows that similar phenomena are produced, except with a clock-wise rotation. Asymmetric photoelectron angular and momentum distributions resulting from the coherent excitation by the $\lambda_{pu} = 70$ nm pump pulse are produced as well. Varying the time delay $\Delta\tau$ gives rise to a periodical rotation of photoelectron distributions with period 232 as, as predicted in Equation (10). It is found that the rotation with a clock-wise direction follows the right handed helicity of the circularly polarized probe pulse. The combination of Figures 4 and 5 shows that the evolution of the probing photoelectron angular and momentum distributions with time arises from the coherent excitation between the ground and excited electronic state by the pump pulse while the rotation corresponds to the helicity of the circularly polarized attosecond probe pulse.

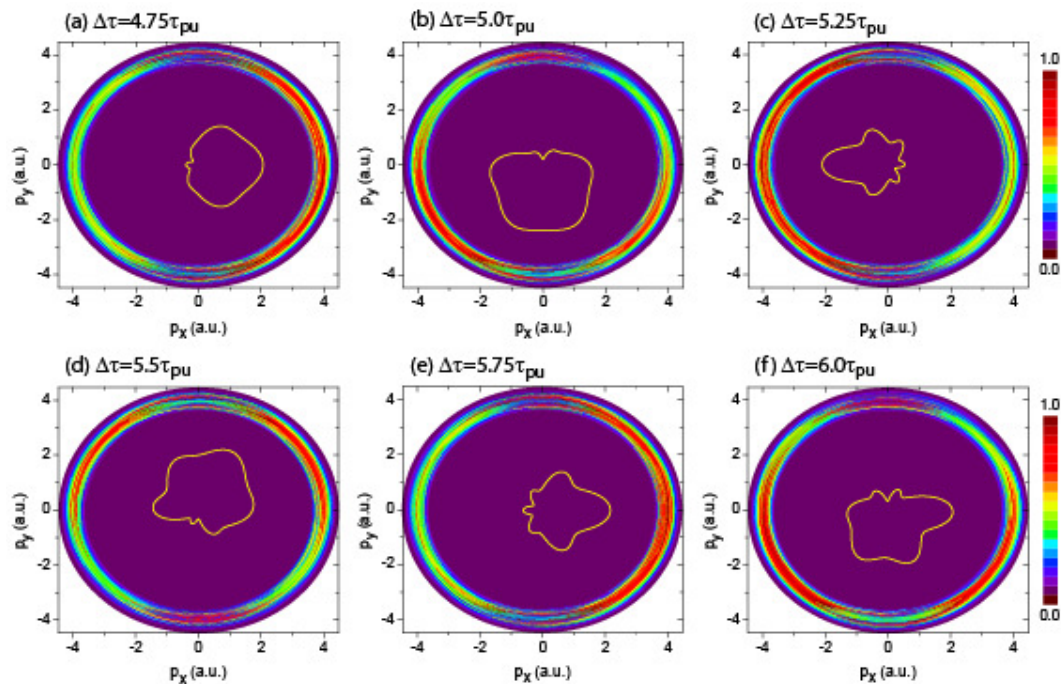


Figure 5. Photoelectron momentum $\mathcal{J}(p_x, p_y)$ distributions as functions of the time delay $\Delta\tau$ between the linearly x polarized $\lambda_{pu} = 70$ nm pump pulse and the circularly (x, y) polarized $\lambda_{pr} = 5$ nm probe pulse with right-handed helicity $\zeta = 1$. The time delay $\Delta\tau$ varies: (a) $4.75\tau_{pu}$; (b) $5.0\tau_{pu}$; (c) $5.25\tau_{pu}$; (d) $5.5\tau_{pu}$; (e) $5.75\tau_{pu}$; and (f) $6.0\tau_{pu}$. The molecule H_2^+ is aligned along the z -axis. The pulse intensities $I_0 = 1.0 \times 10^{14}$ W/cm² ($E_0 = 5.34 \times 10^{-2}$ a.u.) and duration $T_{pu} = 10\tau_{pu} = 2.32$ fs (1.16 fs FWHM) and $T_{pr} = 10\tau_{pr} = 165.4$ as (83 as FWHM) are always fixed. Inserts (yellow curves) are photoelectron angular $\mathcal{J}(\theta)$ distributions obtained from Equation (6).

Comparison of results in Figures 3–5 shows that the time-resolved photoelectron angular and momentum distributions depend on the polarization and helicity of the probe pulse. By a linearly polarized pump pulse, the coherent electronic state is degenerate with $m = \pm 1$. The subsequent ionization from the coherent superposition state are dependent on the properties of the probe pulse. The evolution of the probing photoelectron angular and momentum distributions with the time delay depends on the polarization and helicity of the soft X-ray probe pulse, as illustrated in Figures 3–5. This differs from the coherent excitation process by a circularly polarized pump pulse, in which the excited $2p\pi_u$ state is non-degenerate, with $m = 1$ or -1 . As we reported previously [43], the rotation of time-delay dependent photoelectron distributions is determined by the pump pulse. Altering the helicity of the probe pulse cannot vary the rotation of the time-resolved photoelectron distribution. The dependence of the time-resolved photoelectron distributions on the polarization and helicity of the soft X-ray probe pulse indicates the permanent property of the coherent superposition state in the coherent excitation and charge migration. Of interest is that, in the present work, we consider the process of molecular resonant excitations with $\sigma_g - \pi_u$ symmetries in the molecular ion H_2^+ . By a

linearly polarized XUV pulse with its field polarized along the x -axis, the $\sigma_g - \pi_u$ transition occurs only in the case of the molecular axis perpendicular to the laser polarization direction. Therefore, only the excitations that are mainly localized along the laser polarization direction dominate the spectrum and evolve periodically with time, as shown in Figure 2. Therefore, the time-dependent signatures of the coherent electronic dynamics can also be observed even when averaging over all molecular alignments.

4. Conclusions

In summary, we present time resolved photoelectron emission in electron coherent excitation and charge migration processes. Simulations were performed on the aligned molecular ion H_2^+ by numerically solving the molecular TDSE. The molecule was excited by a linearly polarized XUV pulse, creating a coherent superposition of the ground and excited electronic states. Subsequently, a linearly/circularly polarized soft X-ray attosecond probe pulse was used to ionize the excited molecule. Probing molecular photoelectron momentum distribution displayed an asymmetric structure, which was shown to be dependent on the time delay between the pump and probe pulses, and the polarization and helicity of the probe pulse.

The asymmetry of the time resolved photoelectron angular and momentum distributions arose from the coherent excitation of the molecule induced by the pump pulse. The dependence of the probing photoelectron emission yield on the time-delay illustrated the evolution of the coherent electron wave packets with time. Our numerical simulations combined with theoretical analysis therefore showed that the time resolved X-ray photoelectron imaging allows monitoring the electron coherence in molecular reaction processes. We showed how the polarization and helicity of the soft X-ray probe pulse influence the probing photoelectron emission, illustrating the property of the coherent superposition state in molecular coherent excitation and charge migration. Relating to new experiments in attosecond time-delayed photoionization of molecules [60], our results pave the way to visualize and manipulate electron motion inside molecules by time-dependent photoelectron spectroscopy imaging, which can be extended to more complex systems and laser control of chemical reactions [61,62].

Author Contributions: K.-J.Y. and A.D.B. conceived and designed the pump–probe photoelectron spectroscopy imaging model; K.-J.Y. performed the numerical simulations; and K.-J.Y. and A.D.B. analyzed the results and wrote the paper.

Funding: This research was funded by the Natural Sciences and Engineering Research Council of Canada (NSERC) and the Fonds de recherche du Québec–Nature et technologies (FRQNT).

Acknowledgments: The authors thank Compute Canada for access to massively parallel computer clusters.

Conflicts of Interest: The authors declare no conflict of interest.

References

1. Zewail, A.H. Femtochemistry: Atomic-Scale Dynamics of the Chemical Bond. *J. Phys. Chem. A* **2000**, *104*, 5660–5694. [[CrossRef](#)]
2. Stolow, A.; Bragg, A.E.; Neumark, D.M. Femtosecond Time-Resolved Photoelectron Spectroscopy. *Chem. Rev.* **2004**, *104*, 1719–1758. [[CrossRef](#)] [[PubMed](#)]
3. Reid, K.L. Picosecond Time-Resolved Photoelectron Spectroscopy as a Means of Gaining Insight into Mechanisms of Intramolecular Vibrational Energy Redistribution in Excited States. *Int. Rev. Phys. Chem.* **2008**, *27*, 607–628. [[CrossRef](#)]
4. Arasaki, Y.; Takatsuka, K.; Wang, K.; McKoy, V. Time-Resolved Photoelectron Spectroscopy of Wavepackets through a Conical Intersection in NO_2 . *J. Chem. Phys.* **2010**, *132*, 124307. [[CrossRef](#)]
5. Douguet, N.; Rescigno, T.N.; Orel, A.E. Time-Resolved Molecular-Frame Photoelectron Angular Distributions: Snapshots of Acetylene-Vinylidene Cationic Isomerization. *Phys. Rev. A* **2012**, *86*, 013425. [[CrossRef](#)]

6. Kammrath, A.; Griffin, G.B.; Verlet, J.R.R.; Young, R.M.; Neumark, D.M. Time-Resolved Photoelectron Imaging of Large Anionic Methanol Clusters: $(\text{Methanol})_n^-$ ($n \sim 145 - 535$). *J. Chem. Phys.* **2007**, *126*, 244306. [[CrossRef](#)] [[PubMed](#)]
7. Svoboda, V.; Ram, N.B.; Rajeev, R.; Wörner, H.J. Time-Resolved Photoelectron Imaging with a Femtosecond Vacuum-Ultraviolet Light Source: Dynamics in the \tilde{A}/\tilde{B} - and \tilde{F} -Bands of SO_2 . *J. Chem. Phys.* **2017**, *146*, 084301. [[CrossRef](#)]
8. Wilma, K.; Shu, C.C.; Scherf, U.; Hildner, R. Two-Photon Induced Ultrafast Coherence Decay of Highly Excited States in Single Molecules. *New J. Phys.* **2019**, *21*, 045001. [[CrossRef](#)]
9. Krausz, F.; Ivanov, M. Attosecond Physics. *Rev. Mod. Phys.* **2009**, *81*, 163-234. [[CrossRef](#)]
10. Chang, Z.; Corkum, P.; Leone, S.R. Attosecond Optics and Technology: Progress to Date and Future Prospects. *J. Opt. Soc. Am. B* **2016**, *33*, 1081-1097. [[CrossRef](#)]
11. Baum, P.; Krausz, F. Capturing Atomic-Scale Carrier Dynamics with Electrons. *Chem. Phys. Lett.* **2017**, *683*, 57-61. [[CrossRef](#)]
12. Gaumnitz, T.; Jain, A.; Pertot, Y.; Huppert, M.; Jordan, I.; Ardana-Lamas, F.; Wörner, H.J. Streaking of 43-Attosecond Soft-X-Ray Pulses Generated by a Passively CEP-Stable Mid-Infrared Driver. *Opt. Express* **2017**, *25*, 27506-27518. [[CrossRef](#)]
13. Zuo, T.; Bandrauk, A.D.; Corkum, P.B. Laser-Induced Electron Diffraction: A New Tool for Probing Ultrafast Molecular Dynamics. *Chem. Phys. Lett.* **1996**, *259*, 313-320. [[CrossRef](#)]
14. Meckel, M.; Comtois, D.; Zeidler, D.; Staudte, A.; Pavicic, D.; Bandulet, H.C.; Pepin, H.; Kieffer, J.C.; Dorner, R.; Villeneuve, D.M.; et al. Laser-Induced Electron Tunneling and Diffraction. *Science* **2008**, *320*, 1478-1482. [[CrossRef](#)] [[PubMed](#)]
15. Li, Y.; Qin, M.; Zhu, X.; Zhang, Q.; Lan, P.; Lu, P. Ultrafast Molecular Orbital Imaging Based on Attosecond Photoelectron Diffraction. *Opt. Express* **2015**, *23*, 10687-10702. [[CrossRef](#)] [[PubMed](#)]
16. Blaga, C.I.; Xu, J.; DiChiara, A.D.; Sistrunk, E.; Zhang, K.; Agostini, P.; Miller, T.A.; DiMauro, L.F.; Lin, C.D. Imaging Ultrafast Molecular Dynamics with Laser-Induced Electron Diffraction. *Nature* **2012**, *483*, 194-197. [[CrossRef](#)] [[PubMed](#)]
17. Ito, Y.; Wang, C.C.; Le, A.T.; Okunishi, M.; Ding, D.J.; Lin, C.D.; Ueda, K. Extracting Conformational Structure Information of Benzene Molecules via Laser-Induced Electron Diffraction. *Struct. Dyn.* **2016**, *3*, 034303. [[CrossRef](#)] [[PubMed](#)]
18. Peters, M.; Nguyen-Dang, T.T.; Charron, E.; Keller, A.; Atabek, O. Laser-Induced Electron Diffraction: A Tool for Molecular Orbital Imaging. *Phys. Rev. A* **2012**, *85*, 053417. [[CrossRef](#)]
19. Puthumpally-Joseph, R.; Viau-Trudel, J.; Peters, M.; Nguyen-Dang, T.T.; Atabek, O.; Charron, E. Inversion of Strong-Field Photoelectron Spectra for Molecular Orbital Imaging. *Phys. Rev. A* **2016**, *94*, 023421. [[CrossRef](#)]
20. Nguyen-Dang, T.T.; Peters, M.; Viau-Trudel, J.; Couture-Bienvenue, E.; Puthumpally-Joseph, R.; Charron, E.; Atabek, O. Laser-Induced Electron Diffraction: Alignment Defects and Symmetry Breaking. *Mol. Phys.* **2017**, *115*, 1934-1943. [[CrossRef](#)]
21. Weinkauff, R.; Schanen, P.; Yang, S.D.; Soukara; Schlag, E.W. Elementary Processes in Peptides: Electron Mobility and Dissociation in Peptide Cations in the Gas Phase. *J. Phys. Chem.* **1995**, *99*, 11255-11265. [[CrossRef](#)]
22. Weinkauff, R.; Schlag, E.W.; Martinez, T.J.; Levine, R.D. Nonstationary Electronic States and Site-Selective Reactivity. *J. Phys. Chem. A* **1997**, *101*, 7702-7710. [[CrossRef](#)]
23. Cederbaum, L.S.; Zobeley, J. Ultrafast Charge Migration by Electron Correlation. *Chem. Phys. Lett.* **1999**, *307*, 205-210. [[CrossRef](#)]
24. Barth, I.; Manz, J. Periodic Electron Circulation Induced by Circularly Polarized Laser Pulses: Quantum Model Simulations for Mg Porphyrin. *Angew. Chem., Int. Ed.* **2006**, *45*, 2962-2965. [[CrossRef](#)] [[PubMed](#)]
25. Mineo, H.; Yamaki, M.; Teranishi, Y.; Hayashi, M.; Lin, S.H.; Fujimura, Y. Quantum Switching of p-Electron Rotations in a Nonplanar Chiral Molecule by Using Linearly Polarized UV Laser Pulses. *J. Am. Chem. Soc.* **2012**, *134*, 14279-14282. [[CrossRef](#)]
26. Kanno, M.; Kono, H.; Fujimura, Y.; Lin, S.H. Nonadiabatic Response Model of Laser-Induced Ultrafast π -Electron Rotations in Chiral Aromatic Molecules. *Phys. Rev. Lett.* **2010**, *104*, 108302. [[CrossRef](#)]
27. Mignolet, B.; Levine, R.D.; Remacle, F. Charge Migration in the Bifunctional PENNA Cation Induced and Probed by Ultrafast Ionization: A Dynamical Study. *J. Phys. B* **2014**, *47*, 124011. [[CrossRef](#)]

28. Despré, V.; Marciniak, A.; Lorient, V.; Galbraith, M.C.E.; Rouzée, A.; Vrakking, M.J.J.; Lépine, F.; Kuleff, A.I. Attosecond Hole Migration in Benzene Molecules Surviving Nuclear Motion. *J. Phys. Chem. Lett.* **2015**, *6*, 426–431. [[CrossRef](#)] [[PubMed](#)]
29. Shao, H.C.; Starace, A.F. Detecting Electron Motion in Atoms and Molecules. *Phys. Rev. Lett.* **2010**, *105*, 263201. [[CrossRef](#)] [[PubMed](#)]
30. Barth, I.; Manz, J.; Shigeta, Y.; Yagi, K. Unidirectional Electronic Ring Current Driven by a Few Cycle Circularly Polarized Laser Pulse: Quantum Model Simulations for Mg-Porphyrin. *J. Am. Chem. Soc.* **2006**, *128*, 7043–7049. [[CrossRef](#)] [[PubMed](#)]
31. Yuan, K.-J.; Bandrauk, A.D. Monitoring Coherent ElectronWave Packet Excitation Dynamics by Two-Color Attosecond Laser Pulses. *J. Chem. Phys.* **2016**, *145*, 194304. [[CrossRef](#)] [[PubMed](#)]
32. Diestler, D.J.; Hermann, G.; Manz, J. Charge Migration in Eyring, Walter and Kimball's 1944 Model of the Electronically Excited Hydrogen-Molecule Ion. *J. Phys. Chem. A* **2017**, *121*, 5332–5340. [[CrossRef](#)]
33. Wörner, H.J.; Arrell, C.A.; Banerji, N.; Cannizzo, A.; Chergui, M.; Das, A.K.; Hamm, P.; Keller, U.; Kraus, P.M.; Liberatore, E.; et al. Charge Migration and Charge Transfer in Molecular Systems. *Struct. Dyn.* **2017**, *4*, 061508. [[CrossRef](#)]
34. Hu, W.; Liu, Y.; Luo, S.; Li, X.; Yu, J.; Li, X.; Sun, Z.; Yuan, K.J.; Bandrauk, A.D.; Ding, D. Coherent Interference of Molecular Electronic States in NO by Two-Color Femtosecond Laser Pulses. *Phys. Rev. A* **2019**, *99*, 011402. [[CrossRef](#)]
35. Kanno, M.; Kano, H.; Fujimura, Y. Laser-Control of Ultrafast π -Electron Ring Currents in Aromatic Molecules: Roles of Molecular Symmetry and Light Polarization. *Appl. Sci.* **2018**, *8*, 2347. [[CrossRef](#)]
36. Mineo, H.; Lin, S.H.; Fujimura, Y. Coherent p-Electron Dynamics of (P)-2,2'-Biphenol Induced by Ultrashort Linearly Polarized UV Pulses: Angular Momentum and Ring Current. *J. Chem. Phys.* **2013**, *138*, 074304. [[CrossRef](#)]
37. Hermann, G.; Liu, C.; Manz, J.; Paulus, B.; Pérez-Torres, J.F.; Pohl, V.; Tremblay, J.C. Multidirectional Angular Electronic Flux during Adiabatic Attosecond Charge Migration in Excited Benzene. *J. Phys. Chem. A* **2016**, *120*, 5360–5369. [[CrossRef](#)]
38. Hermann, G.; Liu, C.; Manz, J.; Paulus, B.; Pohl, V.; Tremblay, J.C. Attosecond Angular Flux of Partial Charges on the Carbon Atoms of Benzene in Non-Aromatic Excited State. *Chem. Phys. Lett.* **2017**, *683*, 553–558. [[CrossRef](#)]
39. Jia, D.; Manz, J.; Paulus, B.; Pohl, V.; Tremblay, J.C.; Yang, Y. Quantum Control of Electronic Fluxes During Adiabatic Attosecond Charge Migration in Degenerate Superposition States of Benzene. *Chem. Phys.* **2017**, *482*, 146–159. [[CrossRef](#)]
40. Liu, C.; Manz, J.; Ohmori, K.; Sommer, C.; Takei, N.; Tremblay, J.C.; Zhang, Y. Attosecond Control of Restoration of Electronic Structure Symmetry. *Phys. Rev. Lett.* **2018**, *121*, 173201. [[CrossRef](#)]
41. Liu, C.; Manz, J.; Tremblay, J.C. From Symmetry Breaking via Charge Migration to Symmetry Restoration in Electronic Ground and Excited States: Quantum Control on the Attosecond Time Scale. *Appl. Sci.* **2019**, *9*, 953. [[CrossRef](#)]
42. Kraus, P.M.; Mignolet, B.; Baykusheva, D.; Rupenyau, A.; Horný, L.; Penka, E.F.; Grassi, G.; Tolstikhin, O.I.; Schneider, J.; Jensen, F.; et al. Measurement and Laser Control of Attosecond Charge Migration in Ionized Iodoacetylene. *Science* **2015**, *350*, 790–795. [[CrossRef](#)] [[PubMed](#)]
43. Yuan, K.J.; Shu, C.C.; Dong, D.; Bandrauk, A.D. Attosecond Dynamics of Molecular Electronic Ring Currents. *J. Phys. Chem. Lett.* **2017**, *8*, 2229–2235. [[CrossRef](#)] [[PubMed](#)]
44. Popova-Gorelova, D.; Küpper, J.; Santra, R. Imaging Electron Dynamics with Time- and Angle-Resolved Photoelectron Spectroscopy. *Phys. Rev. A* **2016**, *94*, 013412. [[CrossRef](#)]
45. Yuan, K.J.; Bandrauk, A.D. Exploring Coherent Electron Excitation and Migration Dynamics by Electron Diffraction with Ultrashort X-ray Pulses. *Phys. Chem. Chem. Phys.* **2017**, *19*, 25846–25852. [[CrossRef](#)] [[PubMed](#)]
46. Yuan, K.J.; Bandrauk, A.D. Time-Resolved Photoelectron Imaging of Molecular Coherent Excitation and Charge Migration by Ultrashort Laser Pulses. *J. Phys. Chem. A* **2018**, *122*, 2241–2249. [[CrossRef](#)] [[PubMed](#)]
47. Yuan, K.J.; Bandrauk, A.D. Ultrafast X-ray Photoelectron Imaging of Attosecond Electron Dynamics in Molecular Coherent Excitation. *J. Phys. Chem. A* **2019**, *123*, 1328–1336. [[CrossRef](#)] [[PubMed](#)]
48. Simmermacher, M.; Henriksen, N.E.; Møller, K.B.; Carrascosa, A.M.; Kirrander, A. Electronic Coherence in Ultrafast X-Ray Scattering from Molecular Wave Packets. *Phys. Rev. Lett.* **2019**, *122*, 073003. [[CrossRef](#)]

49. Suzuki, T. Femtosecond Time-Resolved Photoelectron Imaging. *Ann. Rev. Phys. Chem.* **2006**, *57*, 555–592 [[CrossRef](#)] [[PubMed](#)]
50. Kunin, A.; Li, W.L.; Neumark, D.M. Dynamics of Electron Attachment and Photodissociation in Iodide-Uracil-Water Clusters via Time-Resolved Photoelectron Imaging. *J. Chem. Phys.* **2018**, *149*, 084301. [[CrossRef](#)]
51. Bandrauk, A.D.; Shen, H. Exponential Split Operator Methods for Solving Coupled Time-Dependent Schrödinger Equations. *J. Chem. Phys.* **1993**, *99*, 1185–1193. [[CrossRef](#)]
52. Bandrauk, A.D.; Lu, H. Exponential Propagators (Integrators) for the Time-Dependent Schrödinger Equation. *J. Theor. Comput. Chem.* **2013**, *12*, 1340001–1340017. [[CrossRef](#)]
53. Krause, J.L.; Schafer, K.J.; Kulander, K.C. Calculation of Photoemission from Atoms Subject to Intense Laser Fields. *Phys. Rev. A* **1992**, *45*, 4998. [[CrossRef](#)]
54. He, F.; Ruiz, C.; Becker, A. Absorbing Boundaries in Numerical Solutions of the Time-Dependent Schrödinger Equation on a Grid using Exterior Complex Scaling. *Phys. Rev. A* **2007**, *75*, 053407. [[CrossRef](#)]
55. Yuan, K.J.; Lu, H.Z.; Bandrauk, A.D. Linear- and Circular-Polarization Photoionization Angular Distributions in H₂ and H₂⁺ by Attosecond XUV Laser Pulses. *Phys. Rev. A* **2011**, *83*, 043418. [[CrossRef](#)]
56. Yuan, K.J.; Lu, H.; Bandrauk, A.D. Molecular Photoelectron Interference Effects by Intense Circularly Polarized Attosecond X-ray Pulses. *Struct. Chem.* **2017**, *28*, 1297–1309. [[CrossRef](#)]
57. Ibrahim, H.; Lefebvre, C.; Bandrauk, A.D.; Staudte, A.; Légaré, F. H₂: the Benchmark Molecule for Ultrafast Science and Technologies. *J. Phys. B* **2018**, *51*, 042002. [[CrossRef](#)]
58. Mulliken, R.S. Low Electronic States of Simple Heteropolar Diatomic Molecules: III. Hydrogen and Univalent Metal Halides. *Phys. Rev.* **1937**, *51*, 310–332. [[CrossRef](#)]
59. Kanno, M.; Kono, H.; Lin, S.H.; Fujimura, Y. Laser-Induced Electronic and Nuclear Coherent Motions in Chiral Aromatic Molecules. In *Quantum Systems in Chemistry and Physics, Progress in Methods and Applications*; Nishikawa, K., Maruani, J., Brändas, E., Delgado-Barrio, G., Piecuch, P., Eds.; Springer: Dordrecht, The Netherlands, 2012; pp. 121–148.
60. Huppert, M.; Jordan, I.; Baykusheva, D.; von Conta, A.; Wörner, H.J. Attosecond Delays in Molecular Photoionization. *Phys. Rev. Lett.* **2016**, *117*, 093001. [[CrossRef](#)]
61. Nisoli, M.; Decleva, P.; Calegari, F.; Palacios, A.; Martin, F. Attosecond Electron Dynamics in Molecules. *Chem. Rev.* **2017**, *117*, 10760–10825. [[CrossRef](#)]
62. Beaulieu, S.; Comby, A.; Clergerie, A.; Caillat, J.; Descamps, D.; Dudovich, N.; Fabre, B.; Généaux, R.; Légaré, F.; Petit, S.; et al. Attosecond-Resolved Photoionization of Chiral Molecules. *Science* **2017**, *358*, 1288–1294 [[CrossRef](#)] [[PubMed](#)]



© 2019 by the authors. Licensee MDPI, Basel, Switzerland. This article is an open access article distributed under the terms and conditions of the Creative Commons Attribution (CC BY) license (<http://creativecommons.org/licenses/by/4.0/>).